PROTEINS: Structure, Function, and Bioinformatics 58:735–746 (2005)

High Affinity Fucose Binding of *Pseudomonas aeruginosa* lectin PA-IIL: 1.0 Å Resolution Crystal Structure of the Complex Combined with Thermodynamics and Computational Chemistry Approaches

Edward P. Mitchell,[1] Charles Sabin,[1,2] Lenka Šnajdrová,[2,3] Martina Pokorná,[3] Stéphanie Perret,[2] Catherine Gautier,[2] Ctirad Hofr,[4] Nechama Gilboa-Garber,[5] Jaroslav Koča,[3] Michaela Wimmerová,[3,6] and Anne Imberty[2,*]

[1]*E.S.R.F. Experiments Division, Grenoble, France*
[2]*CERMAV - CNRS (affiliated with Université Joseph Fourier), Grenoble, France*
[3]*NCBR, Masaryk University, Brno, Czech Republic*
[4]*Institute of Biophysics, Academy of Sciences of the Czech Republic, Brno, Czech Republic*
[5]*Bar-Ilan University, Faculty of Life Sciences, Ramat Gan, Israel*
[6]*Department of Biochemistry, Masaryk University, Brno, Czech Republic*

ABSTRACT **PA-IIL is a fucose-binding lectin from *Pseudomonas aeruginosa* that is closely related to the virulence factors of the bacterium. Previous structural studies have revealed a new carbohydrate-binding mode with direct involvement of two calcium ions (Mitchell E, Houles C, Sudakevitz D, Wimmerova M, Gautier C, Peréz S, Wu AM, Gilboa-Garber N, Imberty A. Structural basis for selective recognition of oligosaccharides from cystic fibrosis patients by the lectin PA-IIL of *Pseudomonas aeruginosa*. Nat Struct Biol 2002;9:918–921). A combination of thermodynamic, structural, and computational methods has been used to study the basis of the high affinity for the monosaccharide ligand. A titration microcalorimetry study indicated that the high affinity is enthalpy driven. The crystal structure of the tetrameric PA-IIL in complex with fucose and calcium was refined to 1.0 Å resolution and, in combination with modeling, allowed a proposal to be made for the hydrogen-bond network in the binding site. Calculations of partial charges using ab initio computational chemistry methods indicated that extensive delocalization of charges between the calcium ions, the side chains of the protein-binding site and the carbohydrate ligand is responsible for the high enthalpy of binding and therefore for the unusually high affinity observed for this unique mode of carbohydrate recognition. Proteins 2005;58:735–746.** © 2004 Wiley-Liss, Inc.

Key words: ***Pseudomonas aeruginosa;*** **lectin; fucose; cristallography; thermodynamics; quantum chemistry**

INTRODUCTION

Pseudomonas aeruginosa is a gram-negative bacterium that is found in various environments including soil, water, and vegetation. It is also an opportunistic pathogen, responsible for numerous nosocomial infections in immunocompromised patients. The bacteria colonize patients suffering from a number of chronic lung diseases, particularly those under assisted ventilation. Their infections are frequently fatal for cystic fibrosis patients. The airway epithelia glycoconjugates and the abundant mucins of CF patients are known to be modified and serve as attachment points for *P. aeruginosa*.[1–3] For this reason, the different carbohydrate-binding proteins of these bacteria (pilin, flagellin, and non-pili lectins) are of high interest for their role in host recognition and specific adhesion. Under certain culture conditions, *P. aeruginosa* expresses two intracellular lectins, PA-IL and PA-IIL, specific for galactose and fucose, respectively.[4] The two lectins consist of four subunits of 12.7 kDa[5] and 11.7 kDa,[6] respectively. These lectins, which do not display sequence similarity, are mainly associated with the inner membrane of the bacteria,[7] but can also be exposed at the surface.[8]

The present study focuses on PA-IIL, the fucose-binding lectin that recently attracted much attention.[9] In hemagglutination inhibition tests, the strongest monosaccharide derivative inhibition was obtained with *p*-nitrophenyl-α-L-fucose followed by L-fucose > L-galactose > D-arabinose > D-fructose, and D-mannose while D-galactose was not active.[10] PA-IIL is characterized by high affinity for L-fucose[10] with an association constant (K_a) of 1.6×10^6 M^{-1}. Such micromolar affinity range is very unusual among lectin-monosaccharide interactions where the millimolar range is more commonly observed. PA-IIL has been the subject of two crystallographic studies[8,11] that yielded

Abbreviations: CF, cystic fibrosis; PA-IL, *Pseudomonas aeruginosa* first (galactose-binding) lectin; PA-IIL, *Pseudomonas aeruginosa* second (fucose-binding) lectin

The Supplementary Materials referred to in this article can be found at http://www.interscience.wiley.com/jpages/0887-3585/suppmat/index.html. Included is a table of charges similar to Table V but for other calculation methods (HF and Mulliken).

*Correspondence to: Anne Imberty, CERMAV-CNRS, 601 rue de la Chimie, BP53, 38042 Grenoble cedex 9, France. E-mail: imberty@cermav.cnrs.fr

Received 4 June 2004; Accepted 13 August 2004

Published online 30 November 2004 in Wiley InterScience (www.interscience.wiley.com). DOI: 10.1002/prot.20330

several structures: in addition to the native lectin and the calcium-free one, complexes with three monosaccharides L-fucose, D-mannose, and D-fructopyranose have been described. In the PA-IIL/fucose complex,[11] the fucose residue locks onto a pair of calcium ions with three of its hydroxyl groups participating in the coordination of these cations. Such a protein/carbohydrate binding mode has never been observed before. The different orientation of mannose and fructose in complex with the lectin[8] yielded isosterical arrangements of three sugar hydroxyl groups in direct contact with the calcium ions. More recently, a sequence-related protein purified from the plant pathogenic bacterium *Ralstonia solananacearum,* RS-IIL, has been cocrystallized with mannose and the structure displays the same peculiar role for a pair of calcium ions in the binding site.[12]

The presence of the two calcium ions in the binding site appears to be the clue for the two particularities of PA-IIL: the weak specificity and the high affinity. The weak specificity has been fully characterized by crystallography and the requirement for the particular stereochemistry of two equatorial and one axial hydroxyl groups is now well established[12] and leads to a number of sugars being able to bind. The aim of the present work was to investigate the high affinity of PA-IIL for fucose. The thermodynamic basis of the affinity has been studied by analyzing enthalpy and entropy contributions while the atomic basis is characterized fully by the 1.0 Å resolution crystal structure of the complex. Further rationalization is brought by the study of charge distribution carried out with ab initio calculations. This combination of structural and thermodynamic approaches could serve for further development of anti-adhesion therapeutics against *P. aeruginosa* infections.

MATERIALS AND METHODS

Construction of Plasmid for Expression of PA-IIL

The oligonucleotides used as primers were as follows: 5′-GGA GAT ACC ATA TGG CAA CAC AAG GAG-3′ (27-mer) and 5′-TTC CAA GCT TCT AGC CGA GCG G-3′ (22-mer). The former is designed for the introduction of NdeI and the latter for HindIII restriction sites, respectively. The PCR was performed by using Taq polymerase (Qiagen, GmbH, Germany) and template DNA from *Pseudomonas aeruginosa* ATCC 33347. After digestion with NdeI and HindIII, the amplified fragment was introduced into multiple cloning site of pET-25(b+) vector (Novagen, Madison, WI) resulting in plasmid pET25pa2l.

Expression and Purification of PA-IIL

E. coli BL21(DE3) cells containing the plasmid pET25pa2l were cultured in 1 L of Luria broth (LB) at 37°C. When the culture reached an optical density of 0.5–0.6 at 600 nm, iso-propyl-β-D-thiogalactopyranoside (IPTG) was added to a final concentration of 0.5 mM. Cells were harvested after 3 h incubation at 30°C, washed and resuspended in 10 ml of the buffer (20 mM Tris/HCl, 100 mM NaCl, 100 μM $CaCl_2$, pH 7.5). The cells were disrupted by sonication (Soniprep 150, Schoeller instruments, GB). After centrifugation at 10,000 g for 1 h, the supernatant was further purified on D-Mannose Agarose (Sigma-Aldrich, USA). PA-IIL was allowed to bind to the immobilized mannose in the equilibrating buffer (20 mM Tris/HCl, 100 mM NaCl, 100 μM $CaCl_2$, pH 7.5) and then was eluted by the elution buffer (20 mM Tris/HCl, 100 mM NaCl, 100 μM $CaCl_2$, 0.1 M mannose, pH 7.5). The purified protein was intensively dialyzed against distilled water for 1 week (for the removal of D-mannose), concentrated by lyophilization and kept at −20°C.

Hemagglutination Activities and Their Inhibition

Samples (0.05 ml) of the native and recombinant PA-IIL solutions, each at a concentration of 1 mg per ml, were serially twofold diluted with 0.05 ml saline. Then 0.05 ml of 5% suspension of papain-treated type O human erythrocytes[4] was added to each tube. Following a short shaking and 30 min at room temperature the tubes were centrifuged for 30 s (1000×) and the hemagglutination was examined. For the inhibition test L-fucose and D-mannose solutions at 0.15 M concentration were serially twofold diluted in 0.05 ml saline for each lectin preparation analysis. 0.05 ml of each lectin preparation at the dilution giving a titer of 1:32 was added to each tube in the respective series. After 30 min at room temperature 0.05 ml of the erythrocyte suspension was added to each tube and the hemagglutinating activity was examined as described above.

Microcalorimetry Experiments

Titration calorimetry experiments were performed using two different systems, a Microcal VP-ITC microcalorimeter (Microcal, Northampton, MA) and CSC4200 (Calorimetry Sciences Corp.), respectively. All titrations were performed in 10 mM Tris.HCl buffer containing 0.1 M NaCl and 1–3 mM $CaCl_2$ at different pH as specified in Table II. Aliquots of 4 or 5 μl of each carbohydrate, dissolved in the same buffer, were added at 4 min intervals into the lectin solution present in the calorimeter cell. In the titrations, the protein concentration in the cell varied from 0.078 to 1 and 0.20 to 0.25 mM for Microcal VP-ITC (cell volume = 1411 μl) and CSC4200 (cell volume = 1300 μl), respectively. The sugar concentration in the 250 μl syringe was 10 to 20 times higher than the protein concentration used in the experiment (typically 1 and 4–5 mM for Microcal VP-ITC and CSC4200, respectively). The temperature of the cell was controlled to 25 ± 0.1°C. Data from a control experiment performed by identical monosaccharide injections into the cell containing only a buffer were subtracted prior to data analysis. Integrated heat effects were analyzed by nonlinear regression using a single site-binding model (Microcal Origin 5.0 and Bindworks 3.0). Fitted data yielded the binding constant (K_b) and the enthalpy of binding (ΔH_b). Other thermodynamic parameters, i.e., changes in free energy, ΔG_b, and entropy, ΔS_b, were calculated from equation

$$\Delta G_b = \Delta H_b - T\Delta S_b = - RT\ln K_b$$

where T is the absolute temperature and R = 8.314 $J.mol^{-1}.K^{-1}$. At least two independent titrations were performed for each ligand tested.

TABLE I. Data Collection and Refinement Statistics

Data Collection and Phasing	
Wavelength (Å)	0.934
Resolution (Å)	1.0
Highest resolution shell (Å)	1.00 − 1.04
Completeness (%)	97.7 (94.3)
Space group	$P2_1$
a, b, c (Å)	52.735, 72.827, 54.747
β (°)	94.21
Measured reflections	706877
Unique reflections	216831
Average multiplicity	3.3 (2.9)
Nb of passes (low and high)	2
R_{Merge} (%)	0.063 (0.228)
Average $I/\sigma(I)$	5.0 (2.8)
Wilson B-factor (Å^2)	6.6
ACORN phasing statistics	
Correlation coefficient	0.38 (166355 medium E reflections)
R factor	0.44 (166355 medium E reflections)
Refinement	
Resolution range (Å)	30–1.0
Nb of reflections	212499
Protein atoms	3308
Residues modelled with multiple locations	27
Water molecules	682 (59 with occupancy 0.5)
Solvent ions	2 sulfate groups
Metal ions	8 Ca^{2+}
Ligands	4 fucose residues
R_{crys}	0.1146
R_{free}	0.1351
Cruickshank's DPI based on maximum likelihood (Å)	0.023
Average B_{iso} (Å)	
All atoms	13.1
Main chain	8.8
Side chain and water	16.7
RMS Deviation from ideality	
Bond (Å)	0.015
Angles (degrees)	1.89
Percent of refl. for R_{free}	3% (4332 reflections)
Residues with alternative conformations	
Double	A31,A41,A46,A60,A62, A68,A77,B29,B46, B53,B68,B77, C13,C29, C59,C77,C82,D13, D41,D66,D68,D77.
Triple	A81,B81,C81,D16,D81.

Crystallization and Data Collection

Lyophilized purified PA-IIL was dissolved in water (10 mg ml^{-1}) in the presence of fucose (250 μg ml^{-1}), and salts ($ZnCl_2$, $CaCl_2$, $MgCl_2$ at 2 mM). Crystallization trials were performed with Hampton crystallization screens I and II (Hampton research, Laguna Nigel, CA) using the hanging drop technique. After optimization of conditions, hanging drops were prepared using 2.5 μl of this preparation and 2.5 μl of the reservoir solution consisting of 1.75 M ammonium sulphate in 0.1 M Tris HCl (pH 8.5), and stored at 20°C. Crystals grew in a rectangular form to maximum dimensions of 0.3 × 0.3 × 0.5 mm^3 after one month. They belong to space group $P2_1$ with unit cell dimensions of a = 52.735 Å, b = 72.827 Å, c =54.747 Å, and β = 94.21° at 100K. The asymmetric unit is a tetramer, corresponding to a V_m 1.75 Å^3 Da^{-1} and a solvent content of 29%.

A crystal was cryo-cooled at 100 K, after soaking it for as short a time as possible in glycerol 25% v/v in the precipitant solution. All data images were recorded on an ADSC Q4R CCD detector (Quantum Corp.) on the fixed energy beamline ID14-2 at the ESRF (Grenoble, France). To avoid the loss of the strongest reflections owing to saturation, two sets of data, at low and high resolution, were collected in that order on the same crystal. For the high resolution data the detector was positioned as close as permitted on ID14-2. This did mean that the full resolution available from the crystal was not collected and resulted in a high resolution bin R_{merge} of 22.8%. Measurements were made at a single X-ray wavelength of 0.934 Å. Data were processed with the HKL Suite[13] and scaled and converted to structure factors using the CCP4 program suite[14] (see Table I for data collection and diffraction data statistics).

Structure Determination

Phasing was performed with ACORN,[15] using only the position of five of the calcium ions from the crystal

structure of PA-IIL/fucose complex previously solved at 1.3 Å resolution.[11] No reflections were omitted for the purposes of calculating the normalized structure factors for input to ACORN. Using the ACORN phases, an initial structure was built automatically using ARP/warp[16] to give 440 residues out of a total of 456 for the asymmetric unit cell. The structure was edited using the program O[17] to add missing residues, calcium ions, and fucose ligands that were clearly defined in the electron density maps. This model was then subjected to 20 cycles of refinement in REFMAC[18] yielding R_{crys} of 20.10% and R_{free} of 21.80%. After several cycles of REFMAC refinement with isotropic *B*-factors, including automatic water molecule placement using ARP/warp, manual rebuilding with O, addition of riding hydrogens in REFMAC, and construction of alternative conformations of side chains, R_{crys} and R_{free} values respectively decreased to 15.91% and 16.89%. In the next stage, refinement including anisotropic B-factors and riding hydrogens on all protein and fucose groups except hydroxyl moieties, was performed with SHELXL.[19] Additional water molecules were placed on the basis of Fo-Fc difference maps. Water molecules were added if the electron density was greater than three sigma and the hydrogen bonding network was sensible. In a number of cases the water molecules, though clearly present, were less than 2.0 Å apart and for these two water molecules, each with an occupancy of 0.5, were positioned in the model.

In order to study the protonated state of the aspartic and glutamic acids in the binding site, the last cycles of refinement were conducted without stereochemical restraints on the carbon-oxygen bond lengths and bond angles of the carboxylate groups. This resulted in a final model of 456 residues with four fucose molecules (one per monomer), eight calcium ions (two per monomer), 682 water molecules of which 59 have a half occupancy, two sulfate ions with R_{crys} of 11.46% and R_{free} of 13.51% at 1.0 Å resolution (Table I). Additionally, the last six cycles of SHELX refinement were performed in parallel without the hydrogen atoms modeled on the fucose ligands in order to create an omit map and give a gauge for visualizing the binding site hydroxyl hydrogens (which had never been modeled during the refinement). Coordinates for the 1.0 Å resolution X-ray structure of PA-IIL/fucose complex have been deposited in the Protein Data Bank[20] with the code 1UZV.

Location of Hydroxyl Groups by Molecular Modeling

The hydrogen bond network in the binding site was built using the molecular graphics package Sybyl.[21] Hydrogen atoms on carbons were added geometrically in their riding position. Hydrogens of carbohydrate hydroxyl groups (O2, O3, O4 and O6) and protein (OG or Ser23) were oriented towards the closer acceptor carboxylate group, when present. Several orientations were tested for the water molecules in order to optimize the resulting hydrogen-bond network. Finally, partial charges were added according to the parameterization developed previously for protein–carbohydrate interactions[22] for the Tripos forcefield[23] and the positions of all hydrogen atoms of the binding site were optimized.

Quantum Chemical Calculations

Quantum-chemical calculations were performed on a selected part of the 1.0 Å crystal structure of PA-IIL/fucose, with hydrogen atoms located as described above. The ligand-site amino-acid residues Asn21, Ser23, G1u95, Asp96, Asp99, Asp101, Asn103, Asp104 from the A-chain and Gly114 (from the B-chain) were included in all the calculations. Two calcium ions, one fucose residue and one water molecule that create a hydrogen-bond bridge between the fucose and the protein were also included.

As the first step, the geometry was optimized to ensure that the X-ray structure would be correctly reproduced by quantum chemical calculations. Because of the size of the system (138 heavy atoms), the initial geometry optimizations were performed by semi-empirical methods. All optimizations were carried out with the program MOPAC2002[24] using eight different combinations of methods and techniques: two semi-empirical methods, AM1[25] and PM3[26,27] were combined with two SCF procedures, conventional or MOZYME, and two optimizers, BFGS or EF. The following optional keywords were used: GEO-OK, MMOK, NOXYZ, and NODIIS. The optimizations were performed with both 1.3 Å and 1.0 Å resolution structures. The data analysis was performed using the program TRITON.[28] The best results, with the lowest RMSD difference between the calculated and X-ray data, were obtained by the combination of PM3/EF with conventional SCF procedure. This procedure was therefore used for optimizing the binding site geometry. In order to render the computation less demanding, all backbone atoms were removed, except for Asn21, replacing the Cα atoms by methyl groups. The population analysis on the ab initio level was performed on the binding site with no hydrogen atoms added on the aspartate and glutamate groups, leading to a net charge of −2 for the system. Identical calculations were repeated for different protonation states, adding one or two hydrogen atoms on selected acetate groups. Mulliken population analysis[29] and the population analysis based on the electrostatic potential (ESP) with the subsequent RESP procedure[30,31] were performed on this reduced binding site model. The population analyses were based on two different single-point ab initio calculations, performed at the HF/6-31G** level, and the DFT B3LYP/6-31G** level. All the ab initio calculations were performed using the program Gaussian98.[32]

Data Mining of Similar Sequences

Blast searches[33] were performed on general databases (www.infobiogen.fr) as well as on microbial databases (http://www.ncbi.nlm.nih.gov/sutils) both at the peptide and DNA sequence levels. When only DNA sequences were available, they were translated starting from the first ATG motif upstream. Peptide sequence alignments were performed using Clustalx[34] and displayed with Genedoc.[35]

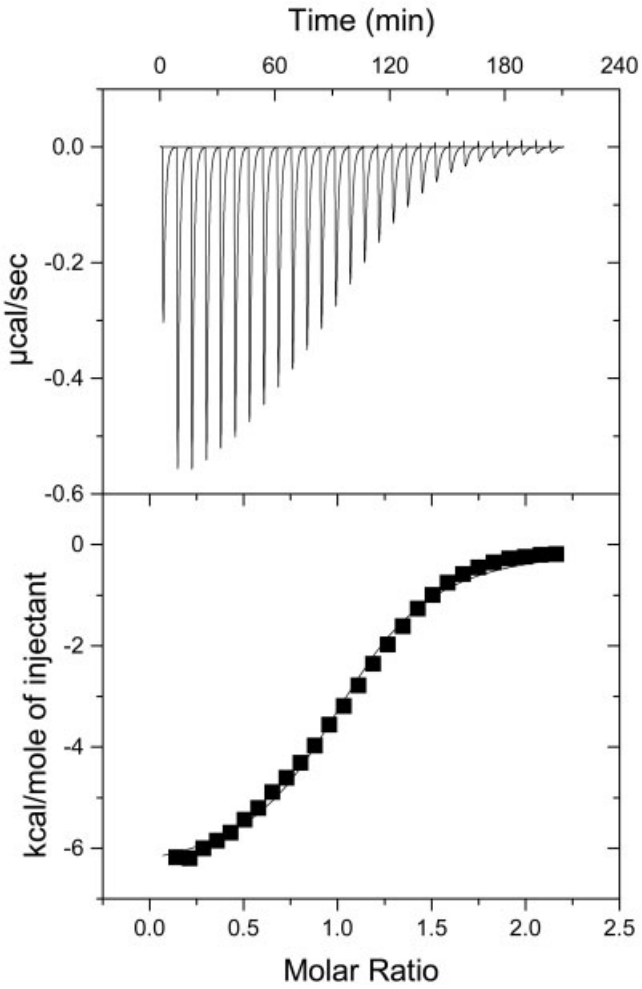

Fig. 1. Titration calorimetry results of L-Fuc (0.78 mM) binding to PA-IIL (0.08 mM) in 10 mM Tris buffer containing 100 mM NaCl and 3 mM $CaCl_2$ (pH 7.5), at 25°C. **Top**: data obtained from 28 automatic injections, 10 µl each, of L-Fuc, into PA-IIL in the cell. **Bottom**: plot of the total heat released as a function of total ligand concentration for the titration shown above (squares). The solid line represents the best least-square fit for the obtained data.

RESULTS

Comparison of Hemagglutination Activity of Recombinant and Native PA-IIL

The hemagglutinating titers of both the native and recombinant lectin preparations were almost the same, 1:256–1:512. The hemagglutination appeared more rapidly with the recombinant lectin. Both lectin preparations also showed similar carbohydrate affinities: being inhibited by fucose dilution up to 0.147mM (11 tubes) and by mannose dilution up to 4.7 mM (5–6 tubes).

Thermodynamic Data

The results of a typical microcalorimetry experiment are displayed in Figure 1, showing a steep decrease in the exothermic heat of binding while saturation is achieved. The values of binding affinity K_b, binding enthalpy ΔH_b and stoichiometry per monomer n have been obtained by fitting a classical equation for single-site binding.[36] The thermodynamic parameters, free energy, and entropy of binding, ΔG_b and ΔS_b, were calculated as indicated in the experimental section. The data obtained under different experimental conditions are listed in Table II. Depending on the pH and conditions of measurement, the binding affinity varied between 120 to 180 10^3 M^{-1}, corresponding to dissociation constants ranging between 5.6 to 8.3 10^{-6} M.

The experiments performed on the CSC and MicroCal calorimeters gave slightly different values for the stoichiometry of the interaction. While an occupancy of almost one fucose per monomer was measured on the Microcal, for the other machine only 75% saturation was obtained. This could be ascribed either to some defects in the protein preparation, with one monomer inactivated, or to problems due to the need of higher protein concentration and/or due to the lower sensitivity of the CSC microcalorimeter. Nevertheless, this does not affect the evaluation of the thermodynamic parameters. In all measurements, a high enthalpy of binding ($\Delta H_b \approx -27.5$ kJ/mol) was observed. The entropy contribution is weak but slightly favorable ($T\Delta S_b \approx 2$ kJ/mol), contributing to less than 7% of the free energy of binding ($\Delta G_b \approx -29.5$ kJ/mol).

Analysis of the Binding Site in the Very High Resolution Crystal Structure

The crystal structure of the PA-IIL/fucose complex refined at 1.0 Å resolution displayed the same overall features [Fig. 2(A)] as those previously refined at 1.3 Å resolution in the same $P2_1$ space group[11] and refined at 1.2 Å resolution in $P2_12_12_1$ space group.[8] In addition to the eight calcium ions, and four fucose ligands, 682 water molecules and two sulfate ions have been refined; 27 amino acids were modeled with two or three conformations.

Each monomer is characterized by a calcium and fucose binding site made up primarily by one long beta-hairpin loop with the participation of a shorter loop and of the C-terminal acidic group at Gly114 of the neighboring monomer. The high resolution allows a detailed analysis of the site. Distances of interest for both the coordination of the two calcium ions, both hepta-coordinated, and the binding of fucose are given in Table III. The two calcium ions are very close to each other, with distances varying from 2.73 to 2.75 Å in the four monomers.

Figure 2(B) illustrates the quality of the electron density map at the ligand site. The omit Fo–Fc difference map allows all of the aliphatic hydrogen atoms of fucose to be located. The difference map contour around the hydrogen at C-1 also indicates that a minority population of fucose adopts the β-configuration, though this was not modeled. The hydroxyl hydrogen atoms are of the greatest interest since they are involved in the hydrogen-bond network between the fucose residue and the protein side chain. Unfortunately only one of three hydroxyl groups can be oriented from the density map. As seen in Figure 2(B), the hydrogen atom of the O-2 hydroxyl group points towards oxygen OD1 of the Asp96 side chain.

Since not all hydrogen atoms can be identified clearly, it is not possible to conclude from the X-ray electron density maps alone the protonation state of the acidic groups

TABLE II. Thermodynamics—ITC for PA-IIL with Fucose[†]

	pH	Calcium (mM)	Kb 10^5 M^{-1}	n	−ΔG (kJ/mol)	−ΔH (kJ/mol)	−ΔS (J/mol. K)	−TΔS (kJ/mol)
Exp 1—fucose[a]	7.4	4	1.2 (± 0.1)	0.78 (± 0.02)	29.0 (± 0.1)	27.7 (± 0.5)	−4.1 (± 1.8)	−1.3 (± 0.5)
Exp 2—fucose[a]	8.5	1–3	1.6 (± 0.2)	0.79 ± (0.06)	29.6 (± 0.3)	27.5 (± 1.4)	−7.1 (± 3.7)	−2.1 (± 0.1)
Exp 3—fucose[b]	7.5	3	1.8 (± 0.2)	1.05 ± (0.02)	29.9 (± 0.2)	27.3 (± 0.3)	−5.9 (± 1.7)	−2.6 (± 0.4)

[†]Experiments 1 to 3 have been conducted using different batches of recombinant protein. Values in parentheses are standard deviations from at least two separate titrations.
[a]Data from CSC ITC microcalorimeter.
[b]Data from a Microcal VP-ITC microcalorimeter.

TABLE III. Geometrical Details of the Four Binding Sites (Distances in Å) in the 1.0-Å Resolution Crystal Structure of PA-IIL/Fucose Complex[†]

		Chain A	Chain B	Chain C	Chain D
Interactions between the calcium ions and the protein.					
Ca-1	Asp101.OD1	2.37	2.37	2.37	2.36
Ca-1	Glu95.E1	2.46	2.46	2.48	2.45
Ca-1	Glu95.E2	2.41	2.42	2.42	2.41
Ca-1	Asp99.OD1	2.36	2.36	2.37	2.38
Ca-1	Asp104.OD2	2.42	2.41	2.41	2.41
Ca-2	Asn21.O	2.38	2.39	2.37	2.39
Ca-2	Asp101.OD2	2.41	2.41	2.42	2.43
Ca-2	Asn103.OD1	2.34	2.34	2.33	2.33
Ca-2	Asp104.OD1	2.35	2.35	2.36	2.34
Ca-2	Gly114.O[a]	2.42	2.44	2.43	2.41
Interactions between the calcium ions and the fucose residue.					
Ca-1	O2	2.51	2.49	2.51	2.48
Ca-1	O3	2.47	2.48	2.48	2.48
Ca-2	O3	2.48	2.49	2.50	2.46
Ca-2	O4	2.49	2.51	2.48	2.50
Direct interactions between the fucose residue and the protein.					
O2	Asp96.OD1 ***	2.67	2.66	2.62	2.66
O3	Asp99.OD1	2.98	3.00	2.94	3.00
O3	Asp99.OD2 ***	2.55	2.57	2.55	2.58
O3	Asp101.OD1	2.95	2.94	2.96	2.96
O3	Asp101.OD2	2.94	2.94	2.94	2.92
O3	Asp104.OD2	2.99	3.01	3.02	2.99
O4	Asn21.O	3.01	3.11	3.07	3.03
O4	Gly114.OXT[a]***	2.53	2.55	2.58	2.58
O5	Ser23.N ***	2.92	2.96	2.95	2.98
C-Me	Thr45.CG2	4.06	4.27	4.09	4.07
Interactions between the fucose residue and the protein via water molecules.					
O1	Wat_1 ***	3.16	3.27	3.13	3.27
O2	Wat_1 ***	3.00	3.04	3.13	3.04
O1	Wat_2 ***	2.76	2.70	2.75	2.76
Wat_1	Thr98.N ***	2.90	2.97	2.90	2.93
Wat_1	Asp99.N ***	3.32	3.18	3.28	3.16
Wat_2	Ser23.OG ***	2.68	2.71	3.32	2.62

[†]The three stars indicate distances with geometrical feature in agreement with existence of a hydrogen bond.
[a]C-terminal residue from the other monomer.

involved in ligand binding. Nevertheless, due to the high resolution of the data (around 5.6 observation per parameter during anisotropic *B*-factor refinement), it was possible to perform 20 refinement cycles without stereochemical restraints on the bond lengths of the COO groups in the ligand site and to analyze the differences, if any. There are few differences between the four monomers of the asymmetric unit, and therefore only the average bond lengths are listed in Table IV. Larger average bond length differences are observed for Asp99 (1.22 Å for CD-OD1 vs. 1.27 Å for CD-OD2). This can be compared to values of 1.24 and 1.32 Å observed for COOH observed in the atomic resolution endocellulase crystal structure.[37] The C-O bonds of the fucose site carboxylates, bar Asp99, refine to lengths between 1.25 and 1.27 Å which are compatible with no protonation of those groups (the estimated average coordinate error being 0.023 Å). Further comparison of the molecular model with the protonated structure of the binding site, as treated by computational chemistry approaches are discussed below.

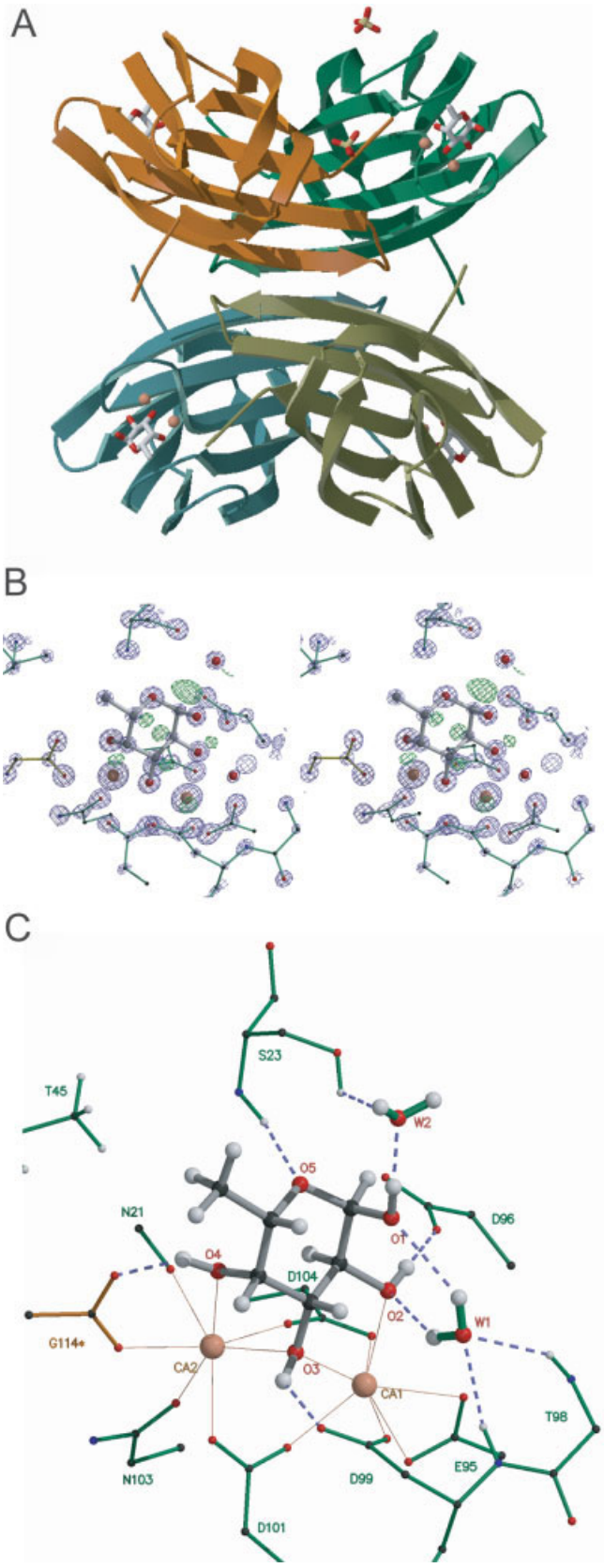

Modeling of Hydrogen-Bond Network

Where it is assumed, accordant with the X-ray data, that none of the aspartate and glutamate side chains of the binding site are protonated, the modeling study arrives at only one possible network of hydrogen bonds between the sugar and the protein. The most buried hydroxyl groups of fucose, i.e., O3 and O4, donate a hydrogen bond to Asp99.OD2 and Gly114*.OXT, respectively. The third hydroxyl group, O2, also donates a hydrogen bond to an acidic group, i.e., to OD1 of Asp96, this hydrogen bond being the only one that could be identified from the X-ray data. With the participation of the backbone NH of Ser23, that gives a hydrogen to the fucose ring oxygen O5, this gives a total of four direct hydrogen bonds that can be modeled unambiguously between the protein and the sugar [Fig. 2(C)]. The hydrogen atoms of the conserved water molecule Wat1 could also be modeled: the orientation of the water molecule could be deduced from the facts that it receives two hydrogens from NH of Thr98 and Asp99 and that it donates one hydrogen to the O2 hydroxyl of fucose. The second hydrogen of the same water molecule can then point to O1 of fucose. The special location of this water molecule seems to allow the water to stabilize the tip of the calcium-carbohydrate binding loop made up of 14 amino acids in a beta-hairpin motif. This particular water is conserved in all PA-IIL/fucose complexes (all four monomers, 1.3 and 1.0 Å resolution). Its special role in maintaining the conformation of the loop is illustrated by the fact that it is also conserved in the native PA-IIL structure, but not in the demetallized one, in which the calcium-binding loop is partially disordered.[8]

The second water molecule, Wat2, that stabilizes the alpha configuration of fucose by bridging the anomeric oxygen atom to the side chain of Ser23 is not so well conserved in all monomers and splits in two close sites (modeled at 0.5 occupancy each) in one of them. As a consequence, there are several possibilities for orienting the protons between the Ser23.OG, Wat2 and O1 of fucose and the network shown in Figure 2(C) represents only one possibility.

The proposed network displayed in Figure 2(C) results in the formation of seven direct or indirect hydrogen bonds between one monosaccharide and the protein.

Fig. 2. Structure of the 1.0 Å resolution structure of the PA-IIL/fucose complex. **A**: Ribbon representation of the tetramer consisting of the asymmetric unit with stick representation of sugar and sulfate and cpk representation of the calcium ions. **B**: Final sigma weighted $2F_o–F_c$ electron density map (blue color contoured at 4 σ) around the monosaccharide residue, water molecules and calcium ions and sigma weighted $F_o–F_c$ omit map (green color contoured at2.5 σ) after six cycles of refinement omitting the hydrogen atoms riding the fucose carbons. **C**: Interactions of PA-IIL with calcium ions and fucose with modeled hydrogen atoms. Coordination contacts are indicated by orange solid lines and hydrogen bonds by green dashed lines. The * symbol indicates the terminal glycine from the other monomer. All molecular drawings were prepared with MOLSCRIPT[53] and RASTER-3D.[54]

TABLE IV. Carbon–Oxygen Bond Lengths in PA-IIL Binding Site[†]

			Length from ab initio calculations, Å			
Residue	C—O bond	Length from X-ray data Å[a]	Non-protonated	Gly114*-protonated	Asp96-protonated	Both protonated
N21	O	1.25	1.23	1.23	1.23	1.23
N103	OD1	1.23	1.24	1.24	1.24	1.25
G114	O	1.27	1.25	1.25	1.25	1.25
	OXT	1.27	1.26	**1.33**[b]	1.26	**1.33**[b]
E95	OE1	1.26	1.27	1.27	1.27	1.27
	OE2	1.27	1.27	1.27	1.28	1.28
D96	OD1	1.25	1.27	1.26	**1.34**[b]	**1.34**[b]
	OD2	1.26	1.25	1.26	1.22	1.22
D99	OD1	1.22	1.27	1.27	1.28	1.27
	OD2	1.27	1.26	1.26	1.25	1.26
D101	OD1	1.26	1.27	1.27	1.27	1.28
	OD2	1.25	1.27	1.28	1.27	1.28
D104	OD1	1.25	1.28	1.29	1.27	1.28
	OD2	1.27	1.27	1.26	1.27	1.26

[†]Comparison between crystallographic data and models calculated using semi-empirical methods for different protonation states.
[a]Average over the four monomers. Standard deviations less than 0.02 Å.
[b]Protonated oxygen atom.

Prediction of Protonation State by Ab Initio Calculations

As described above, the PA-IIL binding site is characterized by the presence of six carboxylate groups that are involved in the binding of two calcium ions. Since there are no amino acids that are likely to be positively charged in the close vicinity of the binding site and assuming zero protonation of the carboxyl groups, the overall charge of the site is expected to be −2. In order to confirm the crystallographic data indicating the absence of protonation, semi-empirical calculations were performed on the binding site in different ionization states. The following residues could potentially be protonated: Glu95, Asp96, Asp99, Asp101, Asp104, and Gly114B. Since both oxygens of Glu95, Asp101, and Asp104 are coordinated by calcium ions, they were excluded. Also Asp99 is unlikely to be protonated because the only position of a hydrogen would be in steric hindrance with O3 hydroxyl group of fucose. Therefore, the most probable candidates for protonation are the C-terminus carboxylate of Gly114B and the Asp96 residue. Four different systems were constructed and optimized: the fully deprotonated structure (i.e., none of the carboxyl groups of the binding site was protonated) with a net charge of −2, two systems with net charges of −1 (one with Gly114B protonated, the other with Asp96 protonated), and one system with a zero net charge (with both Gly231 and Asp96 protonated). In all the above calculations, the original X-ray structure was correctly reproduced with low RMSD (see Table IV) except for the structural details described below. Analysis of the resulting geometries (Table IV) indicates that the computed C–O bond lengths are indeed dependent upon the protonation state with bond length varying from 1.27 (+/−0.03) Å for a delocalized carboxylate C-O bond to 1.33 (+/−0.01) Å for a carboxylic C-OH bond. These lengths can be compared readily to the experimentally measured values in very high resolution crystal structure of endocellulase that contains one protonated glutamate with C-O and C-OH distances of 1.24 and 1.32 Å, respectively.[37] Comparison of the X-ray derived distances with the calculated ones indicates that only the calculation performed without any protonation is in agreement with experimental values. The binding site has been therefore considered as nonprotonated for the rest of the study.

Calculation of Charge Distribution by Ab Initio Calculations

Charge distribution has been calculated on a mini-model of the site as described in the experimental section. Mulliken and RESP charges were calculated using various methods and levels of theory and on different systems: isolated fucose, the binding site of PA-IIL without any ligand, the binding site of PA-IIL with two Ca^{2+} ions and, finally, the binding site of PA-IIL with two Ca^{2+} ions and either a fucose residue or three water molecules (the water molecules replacing the O2, O3, and O4 atoms of fucose) (Table V). The Mulliken scheme does not separate greatly the above different scenarios of the binding site (data in Supplementary Material). However, when the RESP procedure is applied, the charge distribution is very dependent on the composition of the complex. Results obtained by taking RESP charges from B3LYP/6-31G** calculations and from HF/6-31G** calculations are listed in Table V. The complete results, including all data, are provided in supplementary material.

The atomic charges calculated with B3LYP or with HF/6-31G** calculations are in good agreement. When there is no ligand present in the binding site, the global charge of −6 is distributed mainly over the carboxyl groups. When including two calcium ions in the system, highly negative charges are induced in their neighborhood (i.e., on oxygen atoms of carbonyl and carboxyl groups). The calcium ions themselves keep relatively high positive charges of about +1.5. On the other hand, isolated fucose

TABLE V. Charge Distribution in the Binding Site Calculated on Different Systems, Using B3LYP//6–31G (HF/6–31G** in Italics) Ab Initio Calculations with RESP Charges**

	PA-IIL/Ca2+ Fucose	PA-IIL/Ca2+ Water	PA-IIL/Ca2+	Isolated molecule
Protein				
Asn21.O	−0.36/*−0.44*	−0.42/*−0.50*	−0.45/*−0.56*	*−0.32*[a]
Gly114.O	−0.46/*−0.56*	−0.56/*−0.65*	−0.67/*−0.78*	*−0.54*
Asn103.OD1	−0.52/*−0.60*	−0.51/*−0.63*	−0.61/*−0.72*	*−0.56*
Asp99.OD1	−0.67/*−0.78*	−0.74/*−0.87*	−0.82/*−0.93*	*−0.64*
Asp104.OD1	−0.42/*−0.52*	−0.60/*−0.72*	−0.77/*−0.90*	*−0.65*
Asp101.OD1	−0.50/*−0.61*	−0.58/*−0.70*	−0.65/*−0.77*	*−0.51*
Asp101.OD2	−0.65/*−0.76*	−0.69/*−0.81*	−0.76/*−0.87*	*−0.81*
Ca^{2+} ions				
Ca1	1.08/*1.19*	1.33/*1.49*	1.48/*1.62*	
Ca2	0.61/*0.71*	0.99/*1.18*	1.48/*1.64*	
Fucose				
Fuc.O2	−0.18/*−0.24*			−0.52/*−0.60*
Fuc.O3	0.02/*0.01*			−0.49/*−0.57*
Fuc.O4	0.00/*−0.03*			−0.52/*−0.60*
Water				
Wat2		−0.73/*−0.84*		
Wat3		−0.35/*−0.46*		
Wat4		−0.54/*−0.67*		

[a]B3LYP/6–31G** calculations on isolated protein binding site did not converge.

is a neutral molecule but displays rather negatively charged hydroxy-oxygens with partial charges of about −0.5. When two calcium ions and fucose are present in the binding site, the charges on both calcium ions decreases significantly (by about 0.6 to 0.9). A strong charge transfer from three oxygen atoms of fucose and also from the neighboring oxygen atoms of amino acids in the binding site to calcium ions occurs. The situation is somewhere "in between" when there are three water molecules coordinated on calcium ions instead of three oxygens of fucose (see Table V).

In summary, when fucose is not present in the active site, the calcium ions bind by ionic bonds. In this case, the solvent molecules should be very competitive since the free energy of Ca ion solvation is −381 kcal/mol.[38] This would suggest that there is no strong structural role of Ca ions in the unliganded PA-IIL. The fucose binding can be considered as an aqua-substitution reaction for the calcium ion: the fucose hydroxyl groups have a larger mean polarizability than water molecules, resulting in a larger charge redistribution upon binding. In this case, the binding is very strong and this suggests that the Ca ions have a significant structural role in the complex as the charge delocalization is crucial for its stability. Also, the binding site of the protein is stabilized by charge delocalization. It is interesting that when fucose is present, the charge transfer is not as significant on calcium 1 (charge 1.08) as it is on calcium 2 (charge 0.61). This may be caused by the difference in the functional groups that surround the ions and contribute differently to charge delocalization. While calcium 2 is coordinated by oxygens of three carboxyl groups, two carbonyl groups and two oxygens from fucose, calcium 1 is coordinated by oxygens of five carboxyl groups and two oxygens of fucose. So the real difference is the presence of two carbonyl groups which replace two carboxyl groups.

Search for Similar Sequences in Databases

With the rapid progress of bacterial genomics, genes coding for PA-IIL-like proteins were identified in the newly sequenced genome of other bacteria: *Ralstonia solanacearum*,[39] *Chromobacterium violaceum*[40] and *Burkholderia cenocepacia* (The Sanger Institute, unfinished sequence data were obtained from http://www.sanger.ac.uk/Projects/B_cenocepacia/). A similar gene is also present in the newly sequenced genome of another strain of *Pseudomonas aeruginosa*, UCBPP-PA14 (Harvard Partners Center for Genetics and Genomics, http://www.hpcgg.org:8080/hpcgg/jsp/hpcgg/Sequence/mouse/pseudomonas.jsp). The gene product, protein accession number ZP_00136733.1, is apparently shorter at the N-terminus then the protein from *P. aeruginosa* PA01. Detailed analysis of nucleotide sequence prior to the gene sequence revealed that an alternative initiation GTG codon for the automatic gene annotation was taken into account, not considering a presence of the classical initiation ATG codon 15 bp upstream. Moreover, 11 bp further upstream of this new ATG translational start site, a putative Shine-Delgarno sequence can be found, confirming that five amino acids in the annotated gene ZP_00136733.1 are missing. The corrected N-teminus sequence results in complete homology of both *P. aeruginosa* lectins. The alignment of the PA-IIL like region of all the identified and putative lectins is given in Figure 3. In all cases, the PA-IIL-like domain corresponds to the C-terminus, finishing with a fully conserved WPLG sequence. The calcium and sugar binding loop (Asp96 to Asp104 in PA-IIL) is also highly conserved. Four of the sequences, i.e., the ones from both strains of *P. aeruginosa,* from *R. solanacearum,* and from *C. violaceum,* have very similar lengths and almost similar N-term sequences, while the three *B. cenocepacia* sequences have

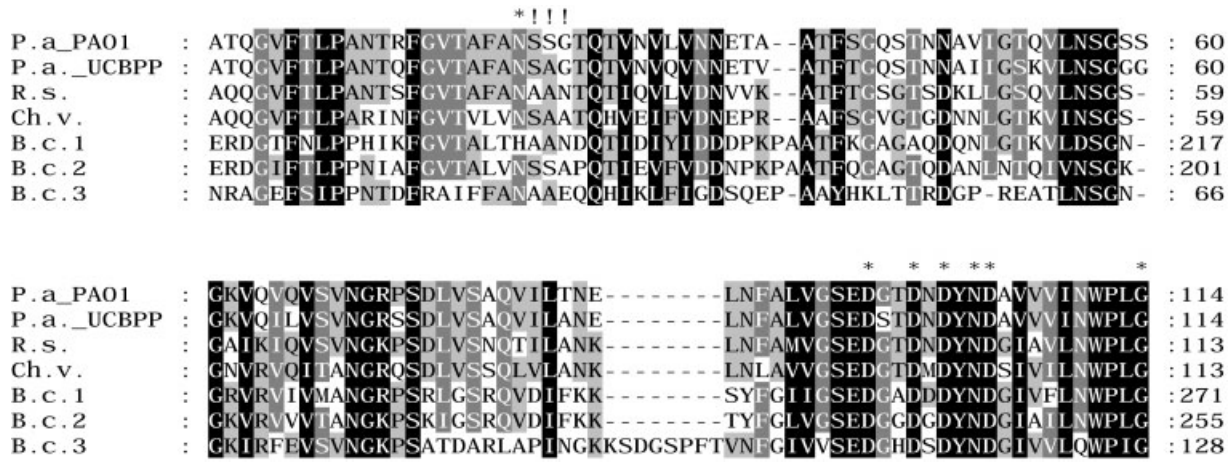

Fig. 3. Alignment of PA-IIL-like sequences from different bacteria. The sequences are from the following genes, with their NCBI/EMBL deposition number between [brackets]. **P.a_PA01**, fucose-binding lectin from *Pseudomonas aeruginosa* PA01 [TrEMBL: Q9HYN5]; **P.a_UCBPP**, ORF Paer104401 from *Pseudomonas aeruginosa* UCBPP-PA14 [NCBI: ZP_00136733.1GI 32038461]; **R.s.**, mannose-binding lectin from *Ralstonia solanacearum* GMI1000 [TrEMBL: Q8XUA5]; **Ch.v.**, ORF CV1744 from *Chromobacterium violaceum* ATCC12472 [NCBI: NP_901414.1 GI:34495455]; **B.c.1**, **B.c.2** and **B.c.3**, ORFs predicted from unfinished sequence data of *Burkholderia cenocepacia* J2315 [chromosome 2, complement: 215683-216501, 214786-215556 and 216624-217013]; Numberings of amino acids is putative for P.a_UCBPP, Ch.v. and the three B.c. and correspond to the most probable limits of the ORF. PA-IIL residues involved in calcium binding are marked by an asterisk and the ones responsible for the fine monosaccharide preference are indicated by an exclamation mark.

longer and more variable N-term regions with no similarity with known proteins (data not shown here).

DISCUSSION

Thermodynamic Basis of PA-IIL Affinity to Fucose

The present microcalorimetry study confirms the very high affinity of the PA-IIL for fucose, albeit with values one order of magnitude lower than that published previously from equilibrium dialysis study (Ka : 1.5 10^6 M^{-1}).[10] The discrepancies between theses values could be due to differences between methodological approaches or between the protein samples. Nevertheless, a review of lectin–protein interactions indicates that the affinity measured here is much higher than the millimolar range usually observed for binding unsubstituted monosaccharides,[41] the highest reported value being a Ka of 9 10^3 M^{-1} for the binding to GalNAc of soybean agglutinin.[42]

Analysis of the different thermodynamic contributions demonstrates that the above interaction is characterized by a strong enthalpy of binding, accompanied by a weakly favorable entropy term (Table II). When compared to classical millimolar range lectin-monosaccharide interactions, the unusual affinity is explained not only by the relatively high enthalpy of binding, but also by the absence of an entropy barrier.

The favorable entropy of binding is very unusual in protein–carbohydrate complexes where an entropy barrier is generally observed.[41] The barrier is higher for the binding of flexible oligosaccharides, but unfavorable negative entropy contributions are also observed for monosaccharide binding and are generally attributed to the displacement of water molecules from disordered locations in amphiphilic regions of the carbohydrate binding sites to more ordered networks in bulk water solution.[43] Nevertheless, favorable entropy has already been observed for the binding of glucose by *Lens culinaris* lectin[44] and the binding of galactose by *Erythrina corallodendron* lectin.[45] In the latter case, structural studies indicated that the favorable entropy may be due to the release of two tightly bound water molecules upon galactose binding.[46] Similar explanation could apply to the favorable entropy observed in PA-IIL/fucose interaction since three water molecules are tightly bound to calcium in the crystal structure of the native lectin[8] and are replaced by fucose hydroxyl groups in the complex.

Atomic Basis of the PA-IIL Affinity for Fucose

A direct interaction between one calcium atom and a sugar ligand has previously been observed in the carbohydrate recognition domain (CRD) of C-type animal lectins that binds neutral monosaccharides with two equatorial hydroxyl groups such as D-mannose, L-fucose or L-galactose.[47] However, in the C-lectin family, the dissociation constant for monosaccharides is in the millimolar range. Another family of lectins that includes serum amyloid P component (SAP) and C-reactive protein (CRP), contains two close calcium ions involved in binding diverse ligands but it differs from that of PA-IIL since it is only directed to negatively charged carbohydrates.[48]

In the present work, the very particular environment of the two close calcium ions was analyzed. Three of the fucose hydroxyl groups are directly involved in the coordination sphere of the calcium ion. Two of these hydroxyl groups create very strong hydrogen bonds with acetate from protein side chains with an O—O distance of 2.55 (+/−0.02) Å, a value significantly shorter than that currently observed in protein carbohydrate interactions. Furthermore, the acetates that are involved in the hydrogen bonds also coordinate the calcium ions. This yields two peculiar six-membered ring arrangements (—O3—O3H—

D99.OD2—D99.CD—D99.OD1—Ca1— and a similar ring involving O2, Gly114 and Ca2) that could be responsible for the strong charge delocalization shown by the ab initio calculations and could therefore play a major role in the unusually high affinity observed between PA-IIL and the monosaccharide.

Biological Occurrence of this Sugar Binding Mode

The PA-IIL sequence, first identified in 2000, has been reported recently in other phylogenetically related bacteria, the plant pathogen *R. solanacearum* and *C. violaceum*.[12] This latter gram-negative saprophytic bacterium from soil and water is of high interest for biotechnology since it produces diverse antibiotics. It is normally considered as a nonpathogen, although it is occasionally involved in infections and may cause fatal septicemias in human and animals.[49] Using the homology searches described above, three ORFs are described for the first time which code for three proteins containing C-terminal sequences highly similar to PA-IIL in another emerging pathogen, *Burkholderia cenocepacia* (previously *B. cepacia*). In the 1980s, it was found to cause life threatening pulmonary infections in cystic fibrosis patients with complications caused by *B. cepacia* having a mortality rate of 80%.[50] It has to be noted that all amino acids involved in calcium binding are fully conserved in these different proteins, including the C-terminal glycine. All these proteins can therefore be postulated to bind two calcium ions and also to display the same dimeric structure as PA-IIL. On the other hand, some variations are observed in the three-amino-acid motif that is responsible for sugar specificity[12] and it is difficult to predict what will be the highest affinity monosaccharide ligand for each sequence. The occurrence of the PA-IIL sequence in four different bacteria may give some clues as to the function of this lectin. These bacteria share some particularities: they are soil inhabitants, opportunistic pathogens, and highly dangerous once an infection is established. It has been observed that the ORFs of *C. violaceum* that present a close similarity to ORFs of both *R. solanacearum* (17.4%) and *P. aeruginosa* (9.6%) are mostly coding for proteins involved in the interactions of these bacteria with their environment.[40]

CONCLUSION

Two paradigms dictate protein–carbohydrate interactions. The first one is that the efficacy of these interactions in biological processes is due to their multivalency that creates an "avidity" or "Velcro" effect that would compensate the low affinity (i.e., millimolar range) generally observed for each binding site.[51] The second paradigm is that protein/sugar binding is mainly due to two types of interaction: the numerous hydrogen bonds, owing to sugar hydroxyl groups, contribute to the affinity, and the van der Waals interactions, mainly due to stacking of the hydrophobic face of sugar to side chains of aromatic amino acids, are responsible of the specificity.[52] The interaction between PA-IIL soluble bacterial lectin and monosaccharides is clearly of a different type: almost no hydrophobic contact is involved and the interaction displays a higher affinity than other protein–carbohydrate interactions, due to the direct involvement of two cations in the binding.

The very fine present analysis of the interaction gives some clues for the development of high-affinity ligands. Possible routes for a rational design of high-affinity anti-adhesive compounds encompass further stabilization of the charge distribution, enhancement of the hydrophobic interactions that are minimal in the complexes studied to date and rational use of the presence of water molecules. These approaches could yield compounds of therapeutic interest not only against *P. aeruginosa*, but also against several other related dangerous pathogens that use similar lectins for their colonization strategy.

ACKNOWLEDGEMENTS

We thank the ESRF, Grenoble, for access to synchrotron data collection facilities. The work was supported by Ministry of Education (LŠ, MP, JK, MW contract LN00A016), and by Grant Agency (CH, Grant 202/01/D110) of the Czech Republic, by CNRS, by French Ministry of Research ACI Microbiologie program and by Vaincre la Mucoviscidose. Travels and visits between NCBR and CERMAV are supported by a BARRANDE exchange program.

REFERENCES

1. Scharfman A, Degroote S, Beau J, Lamblin G, Roussel P, Mazurier J. *Pseudomonas aeruginosa* binds to neoglycoconjugates bearing mucin carbohydrate determinants and predominantly to sialyl-Lewis x conjugates. Glycobiology 1999;9:757–764.
2. Lamblin G, Degroote S, Perini JM, Delmotte P, Scharfman A, Davril M, Lo-Guidice JM, Houdret N, Dumur V, Klein A, Roussel P. Human airway mucin glycosylation: A combinatory of carbohydrate determinants which vary in cystic fibrosis. Glycoconj J 2001;18:661–684.
3. Roussel P, Lamblin G. The glycosylation of airway mucins in cystic fibrosis and its relationship with lung infection by *Pseudomonas aeruginosa*. Adv Exp Med Biol 2003;535:17–32.
4. Gilboa-Garber N. *Pseudomonas aeruginosa* lectins. Meth Enzymol 1982;83:378–385.
5. Avichezer D, Katcoff DJ, Garber NC, Gilboa-Garber N. Analysis of the amino acid sequence of the *Pseudomonas aeruginosa* galactophilic PA-I lectin. J Biol Chem 1992;267:23023–23027.
6. Gilboa-Garber N, Katcoff DJ, Garber NC. Identification and characterization of *Pseudomonas aeruginosa* PA-IIL lectin gene and protein compared to PA-IL. FEMS Immunol Med Microbiol 2000;29:53–57.
7. Glick J, Garber NC. The intracellular localization of *Pseudomonas aeruginosa* lectins. J Gen Microbiol 1983;9:3085–3090.
8. Loris R, Tielker D, Jaeger K-E, Wyns L. Structural basis of carbohydrate recognition by the lectin LecB from *Pseudomonas aeruginosa*. J Mol Biol 2003;331:861–870.
9. Imberty A, Wimmerova M, Mitchell EP, Gilboa-Garber N. Structures of the lectins from *Pseudomonas aeruginosa*: Insights into molecular basis for host glycan recognition. Microb Infect 2004;6:221–228.
10. Garber N, Guempel U, Gilboa-Garber N, Doyle RJ. Specificity of the fucose-binding lectin of *Pseudomonas aeruginosa*. FEMS Microbiol Lett 1987;48:331–334.
11. Mitchell E, Houles C, Sudakevitz D, Wimmerova M, Gautier C, Peréz S, Wu AM, Gilboa-Garber N, Imberty A. Structural basis for oligosaccharide-mediated adhesion of *Pseudomonas aeruginosa* in the lungs of cystic fibrosis patients. Nat Struct Biol 2002;9:918–921.
12. Sudakevitz D, Kostlanova N, Blatman-Jan G, Mitchell EP, Lerrer B, Wimmerova M, Katcof fDJ, Imberty A, Gilboa-Garber N. A new *Ralstonia solanacearum* high affinity mannose-binding lectin RS-IIL structurally resembling the *Pseudomonas aeruginosa* fucose-specific lectin PA-IIL. Mol Microbiol 2004;52:691–700.

13. Otwinowski Z, Minor W. Processing of X-ray diffraction data collected in oscillation mode. In: Carter CWJ, Sweet RM, editors. Macromolecular Crystallography, Part A. San Diego: Academic Press; 1997. p 307–326.
14. Collaborative computational project number 4. The CCP4 suite: programs for protein crystallography. Acta Crystallogr D Biol Crystallogr 1994;50:760–763.
15. Cowtan KD, Zhang KY. Density modification for macromolecular phase improvement. Prog Biophys Mol Biol 1999;72:245–270.
16. Perrakis A, Morris R, Lamzin VS. Automated protein model building combined with iterative structure refinement. Nat Struct Biol 1999;6:458–463.
17. Jones TA, Zou JY, Cowan SW, Kjeldgaard M. Improved methods for building protein models in electron density maps and the location of errors in these models. Acta Crystallogr A 1991;47:110–119.
18. Murshudov GN, A.A.Vagin, E.J.Dodson. Refinement of macromolecular structures by the maximum-likelihood method. Acta Crystallogr D Biol Crystallogr 1997;53:240–255.
19. Sheldrick GM, Schneider TR. Shelxl: High-resolution refinement. Meth Enzymol 1997;277:319–343.
20. Berman HM, Westbrook J, Feng Z, Gilliland G, Bhat TN, Weissig H, Shindyalov IN, Bourne PE. The Protein Data Bank. Nucleic Acids Res 2000;28:235–242.
21. Tripos Associates, 6.4. 1699 S. Hanley Road, Suite 303, St Louis, MO 63144 USA.
22. Imberty A, Bettler E, Karababa M, Mazeau K, Petrova P, Pérez S. Building sugars: The sweet part of structural biology. In Vijayan M, Yathindra N, Kolaskar AS, editors. Perspectives in Structural Biology. Hyderabad: Indian Academy of Sciences and Universities Press; 1999. p 392–409.
23. Clark M, Cramer RDI, van den Opdenbosch N. Validation of the general purpose Tripos 5.2 force field. J Comput Chem 1989;10: 982–1012.
24. MOPAC, 2002. Tokyo: Fujitsu Limited; 1999.
25. Dewar MJS, Zoebisch EG, Healy EF, Stewart JJP. AM1: A new general purpose quantum mechanical model. J Am Chem Soc 1993;107:3902–3909.
26. Stewart JPP. Optimisation of parameters for semi-empirical methods I. Method. J Comp Chem 1989;10:209–220.
27. Stewart JPP. Optimisation of parameters for semi-empirical methods II. Applications. J Comp Chem 1989;10:221–264.
28. Damborsky J, Prokop M, Koca J. TRITON: graphic software for rational engineering of enzymes. Trends Biochem Sci 2001;26:71–73.
29. Mulliken RS. Electronic population analysis on LCAO-MO molecular wave functions I. J Chem Phy 1955;23:1833–1846.
30. Bayly CI, Cieplak P, Cornell WD, Kollman PA. A well-behaved electrostatic potential based method using charge restraints for deriving atomic charges—the RESP model. J Phys Chem 1993;97: 10269–10280.
31. Cornell WD, Cieplak P, Bayly CI, Kollman PA. Application of RESP charges to calculate conformational energies, hydrogen-bond energies, and free-energies of solvation. J Am Chem Soc 1993;115:9620–9631.
32. Gaussian, 98, Revision A. 9. Pittsburgh: Gaussian, Inc.; 1998.
33. Altschul SF, Madden TL, Schäffer AA, Zhang J, Zhang Z, Miller W, Lipman DJ. Gapped BLAST and PSI-BLAST: a new generation of protein database search programs. Nucleic Acids Res 1997;3389–3402.
34. Thompson JD, Higgins DG, Gibson TJ. CLUSTAL W: improving the sensitivity of progressive multiple sequence alignment through sequence weighting, position-specific gap penalties and weight matrix choice. Nucleic Acids Res 1994;22:4673–4680.
35. Nicholas KB, Jr. NHB, Deerfield DWI. GeneDoc: Analysis and visualization of genetic variation. EMBNEW News 1997;4:14.
36. Wiseman T, Williston S, Brandts JF, Lin LN. Rapid measurement of binding constants and heats of binding using a new titration calorimeter. Anal Biochem 1989;179:131–137.
37. Varrot A, Davies GJ. Direct experimental observation of the hydrogen-bonding network of a glycosidase along its reaction coordinate revealed by atomic resolution analyses of endoglucanase Cel5A. Acta Crystallogr D Biol Crystallogr 2003;59:447–452.
38. Magini M, Tanaka N, Ohtaki H, Tamamushi R. Ions and molecules in solution. Amsterdam: Elsevier; 1983. 97 p.
39. Salanoubat M, Genin S, Artiguenave F, Gouzy J, Mangenot S, Arlat M, Billault A, Brottier P, Camus JC, Cattolico L, Chandler M, Choisne N, Claudel-Renard C, Cunnac S, Demange N, Gaspin C, Lavie M, Moisan A, Robert C, Saurin W, Schiex T, Siguier P, Thebault P, Whalen M, Wincker P, Levy M, Weissenbach J, Boucher CA. Genome sequence of the plant pathogen *Ralstonia solanacearum*. Nature 2002;415:497–502.
40. Brazilian National Genome Project Consortium. The complete genome sequence of *Chromobacterium violaceum* reveals remarkable and exploitable bacterial adaptability. Proc Natl Acad Sci USA 2003;100:11660–11665.
41. Dam TK, Brewer CF. Thermodynamic studies of lectin-carbohydrate interactions by isothermal titration calorimetry. Chem Rev 2002;102:387–429.
42. Gupta D, Cho M, Cummings RD, Brewer CF. Thermodynamics of carbohydrate binding to galectin-1 from Chinese hamster ovary cells and two mutants. A comparison with four galactose-specific plant lectins. Biochemistry 1996;35:15236–15243.
43. Lemieux RU, Delbaere LT, Beierbeck H, Spohr U. Involvement of water in host-guest interactions. Ciba Found Symp 1991;158:231–245.
44. Schwarz FP, Puri KD, Bhat RG, Surolia A. Thermodynamics of monosaccharide binding to concanavalin A, pea (*Pisum sativum*) lectin, and lentil (*Lens culinaris*) lectin. J Biol Chem 1993;268: 7668–7677.
45. Surolia A, Sharon N, Schwarz FP. Thermodynamics of monosaccharide and disaccharide binding to *Erythrina corallodendron* lectin. J Biol Chem 1996;271:17697–17703.
46. Elgavish S, Shaanan B. Structures of the *Erythrina corallodendron* lectin and of its complexes with mono- and disaccharides. J Mol Biol 1998;277:917–932.
47. Drickamer K. Ca(2+)-dependent sugar recognition by animal lectins. Biochem Soc Trans 1996;24:146–150.
48. Thompson D, Pepys MB, Tickle I, Wood S. The structures of crystalline complexes of human serum amyloid P component with its carbohydrate ligand, the cyclic pyruvate acetal of galactose. J Mol Biol 2002;320:1081–1086.
49. Duran N, Menck CF. *Chromobacterium violaceum:* a review of pharmacological and industrial perspectives. Crit Rev Microbiol 2001;27:201–222.
50. Mahenthiralingam E, Baldwin A, Vandamme P. *Burkholderia cepacia* complex infection in patients with cystic fibrosis. J Med Microbiol 2002;51:533–538.
51. Sacchettini JC, Baum LG, Brewer CF. Multivalent protein-carbohydrate interactions. A new paradigm for supermolecular assembly and signal transduction. Biochemistry 2001;40:3009–3015.
52. Vyas N. Atomic features of protein-carbohydrate interactions. Curr Opin Struct Biol 1991;1:732–740.
53. Kraulis P. Molscript: A program to produce both detailed and schematic plots of protein structures. J Appl Crystallogr 1991;24: 946–950.
54. Merrit EA, Murphy ME. Raster3D version 2.0. A program for photorealistic molecular graphics. Acta Crystallogr D Biol Crystallogr 1994;50:869–873.